The First Carrier Phase Tracking and Positioning Results With Starlink LEO Satellite Signals

Letter

This letter shows the first carrier phase tracking and positioning results with Starlink's low earth orbit (LEO) satellite signals. An adaptive Kalman filter based algorithm for tracking the beat carrier phase from the unknown Starlink signals is proposed. Experimental results show carrier phase tracking of six Starlink satellites and a horizontal positioning error of 7.7 m with known receiver altitude.

I. INTRODUCTION

Low earth orbit (LEO) broadband communication satellite signals have been considered as possible reliable sources for navigation by various theoretical and experimental studies [1]–[4]. With SpaceX having launched more than a thousand space vehicles (SVs) into LEO, a renaissance in LEO-based navigation has started. Signals from LEO SVs are received with higher power compared to medium earth orbit where GNSS SVs reside. Moreover, LEO SVs are more abundant than GNSS SVs to make up for the reduced footprint, and their signals are spatially and spectrally diverse.

Opportunistic navigation frameworks with LEO SV signals have drawn attention recently as they do not require additional, costly services or infrastructure from the broadband provider [5]. One major requirement in such frameworks is the ability to draw navigation observables from these LEO SV signals of opportunity. However, broadband providers do not usually disclose the transmitted signal structure to protect their intellectual property. As such, one would have to dissect LEO SV signals to draw navigation observables. A cognitive approach to tracking the Doppler frequency of unknown LEO SV signals was proposed in [6]. However, the aforementioned method cannot estimate the carrier phase, nor it can be adopted here since it requires knowledge of the period of the beacon within the transmitted signal, which is unknown in the case of Starlink LEO SVs.

Manuscript received June 25, 2021; released for publication September 7, 2021. Date of publication September 20, 2021; date of current version April 12, 2022.

DOI. No. 10.1109/TAES.2021.3113880

This work was supported in part by the Office of Naval Research (ONR) under Grant N00014-19-1-2511, in part by the National Science Foundation (NSF) under Grant 1929965, and in part by the U.S. Department of Transportation (USDOT) under Grant 69A3552047138 for the CARMEN University Transportation Center (UTC).

Authors' addresses: Joe Khalife and Mohammad Neinavaie are with the Department of Mechanical and Aerospace Engineering, University of California, Irvine, CA 92697 USA, E-mail: (khalifej@uci.edu; mneinava@uci.edu); Zaher M. Kassas is with Department of Mechanical and Aerospace Engineering, University of California, Irvine, CA 92697 USA, and also with the Ohio State University, Columbus, OH 43210 USA, E-mail: (zkassas@ieee.org). *(Corresponding author: Zaher M. Kassas.)*

This letter develops a carrier phase tracking algorithm for Starlink signals without prior knowledge of their structure.

Recent efforts in carrier synchronization showed the benefit of using Kalman filter (KF) based tracking loops over traditional Costas-based phase-locked loops (PLLs) [7]–[10]. These adaptive methods either 1) update the process noise covariance using the residuals or 2) update the measurement noise covariance using the carrier-to-noise ratio. However, high fluctuations in the process noise covariance may cause the filter to diverge [10]. Moreover, the carrier-to-noise ratio cannot be reliably estimated when the signal structure is unknown, as is the case with Starlink signals.

This letter makes the following contributions. First, the Starlink signals are analyzed and a model suitable for carrier phase tracking is developed. Second, an adaptive KF-based tracking loop is developed where the measurement noise is updated based on a heuristic of the residuals. Third, a demonstration of the first carrier phase tracking and positioning results with real Starlink signals is presented, showing a horizontal position error of 7.7 m with six Starlink SVs.

II. RECEIVED SIGNAL MODEL

In this letter, all signals are represented as complex signals (both in-phase and quadrature baseband components).

A. Starlink Downlink Signals

Little is known about Starlink downlink signals or their air interface in general, except for the channel frequencies and bandwidths. One cannot readily design a receiver to track Starlink signals with the aforementioned information only as a deeper understanding of the signals is needed. Software-defined radios (SDRs) come in handy in such situations, since they allow one to sample bands of the radio frequency spectrum. However, there are the following two main challenges for sampling Starlink signals: 1) the signals are transmitted in *Ku*/*Ka*-bands, which is beyond the carrier frequencies that most commercial SDRs can support, and 2) the downlink channel bandwidths can be up to 240 MHz, which also surpasses the capabilities of current commercial SDRs. The first challenge can be resolved by using a mixer/downconverter between the antenna and the SDR. However, the sampling bandwidth can only be as high as the SDR allows. In general, opportunistic navigation frameworks do not require much information from the communication/navigation source (e.g., decoding telemetry or ephemeris data or synchronizing to a certain preamble). Therefore, the aim of the receiver is to exploit enough of the downlink signal to be able produce raw navigation observables (e.g., Doppler and carrier phase). Fortunately, a look at the FFT of the downlink signal at 11.325 GHz carrier frequency and sampling bandwidth of 2.5 MHz shows nine "carrier peaks," as shown in Fig. 1(a). Furthermore, the waterfall plot in Fig. 1(b) shows that these carrier peaks vary as the Doppler frequency over an 80-s interval. The Doppler frequency was predicted using two-line element (TLE) files.

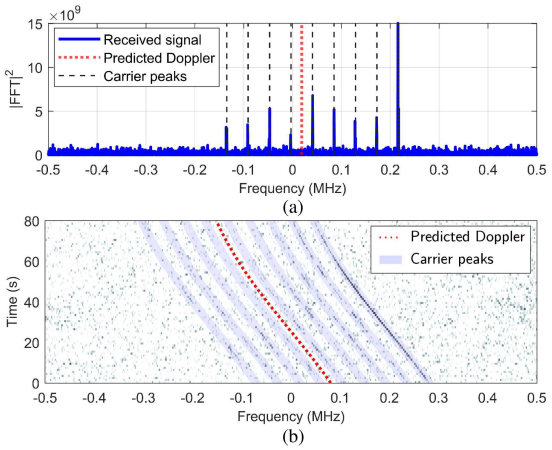

Fig. 1. (a) Snapshot of the square of the FFT of the received signal along with the Doppler frequency predicted using TLEs and the nine observed carrier peaks. (b) Waterfall plot of the FFT of the received signal over an 80-s interval showing the nine peaks varying as the predicted Doppler. The peaks seem to be uniformly separated by approximately 44 kHz.

It was observed that the relative amplitudes of these nine peaks vary from one SV to the other. Therefore, only the strongest peak will be tracked. Moreover, this letter makes no assumptions on the position of the peaks relative to the center frequency of the signal. This results in a Doppler ambiguity that is addressed in the rest of this letter. The following section discusses the assumed transmitted signal model.

B. Continuous-Time Transmitted Baseband Signal Model

Let $x(t)$ denote the continuous-time transmitted signal. As mentioned previously, only one of the nine peaks will be tracked. Motivated by the results in Fig. 1, the transmitted signal $x(t)$ can be modeled as

$$x(t) = \alpha \exp\left[j(2\pi f_p(t - t_0) + \bar{\theta}(t_0)\right] + y(t) \qquad (1)$$

where f_p is the frequency shift of the peak of interest from the center frequency; $\alpha > 0$ is a real, positive amplitude; t_0 is some initial time; $\bar{\theta}(t_0)$ is some initial phase; and $y(t)$ models the remaining components of the transmitted signals. Also, motivated by Fig. 1, the following assumption is made:

$$\frac{1}{\alpha T}\left|\int_t^{t+T} y(\tau)\exp\left[j2\pi(f_p+f)\tau\right]d\tau\right| \ll 1, -\frac{\Delta f}{2} \le f \le \frac{\Delta f}{2} \qquad (2)$$

where Δf is the separation between the peaks and T is the integration period. The assumption in (2) formally states that $y(t)$ is considered as low interference around the peak of interest, which explains the existence of the peaks in Fig. 1(a). The signal $x(t)$ is then mixed to *Ku*-band for transmission.

C. Discrete-Time Received Baseband Signal Model

The Starlink LEO SV's transmitted signal will suffer from very high Doppler shifts, as shown in Fig. 1(b). Note

that ionospheric delays are negligible for the Starlink SV signals in the *Ku*-band. Tropospheric delays are discussed in Section IV-B. After downmixing, low-pass filtering, and bandpass sampling, the nth sample of the discrete-time received signal $r(n)$ can be expressed as

$$r(n) = \alpha \exp\left[j(2\pi f_p n T_s + \bar{\theta}(n))\right] + \beta(n) \tag{3}$$

where T_s is the sampling interval, $\bar{\theta}(n)$ is the true beat carrier phase at time-step n, and β captures the effect of the channel noise and interference and is modeled as a complex, zero-mean white sequence with variance σ_β^2. The Starlink receiver described next will operate on the samples $r(n)$.

III. CARRIER PHASE TRACKING ALGORITHM

It is important to note that the receiver does not have knowledge of f_p. As such, the modified beat carrier phase is defined as $\theta(n) \triangleq \bar{\theta}(n) + 2\pi f_p n T_s$, which will be the quantity tracked by the receiver. Instead of a conventional PLL, an adaptive KF-based tracking loop is developed. The KF formulation allows for arbitrary model order selection, which is crucial in the LEO SVs' high-dynamics. The adaptive KF-based carrier tracking algorithm is described as follows.

A. Beat Carrier Phase Dynamics Model

The time-varying component of the continuous-time true beat carrier phase is a function of 1) the true range between the LEO SV and the receiver, denoted by $d(t)$, and 2) the time-varying difference between the receiver's and LEO SV's clock bias, denoted by $b(t)$ and expressed in meters. Specifically, the modified beat carrier phase can be expressed as

$$\theta(t) = 2\pi\left[-\frac{d(t)}{\lambda} + \frac{b(t)}{\lambda} + f_p(t - t_0)\right] + \bar{\theta}(t_0) \tag{4}$$

where λ is the carrier wavelength. The clock bias is assumed to have a constant drift a, i.e., $b(t) = a \cdot (t - t_0) + b_0$, where b_0 is the initial bias. Moreover, simulations with Starlink LEO SVs show that the following dynamics model for $d(t)$ holds for short periods of time (between carrier phase updates)

$$\dddot{d}(t) = \tilde{w}(t) \tag{5}$$

where $\tilde{w}$ is a zero-mean white noise process with power spectral density $q_{\tilde{w}}$. Subsequently, the kinematic model of the modified beat carrier phase state vector $\boldsymbol{\theta}(t) \triangleq [\theta(t), \dot{\theta}(t), \ddot{\theta}(t)]^\mathsf{T}$ is given by

$$\dot{\boldsymbol{\theta}}(t) = \mathbf{A}\boldsymbol{\theta}(t) + \boldsymbol{b}\tilde{w}(t) \tag{6}$$

$$\mathbf{A} \triangleq \begin{bmatrix} 0 & 1 & 0 \\ 0 & 0 & 1 \\ 0 & 0 & 0 \end{bmatrix}, \quad \boldsymbol{b} \triangleq \begin{bmatrix} 0 \\ 0 \\ \frac{2\pi}{\lambda} \end{bmatrix}$$

and the initial state is given by $\boldsymbol{\theta}(t_0) = [\bar{\theta}(t_0) + \frac{2\pi}{\lambda}(b_0 - d(t_0)), 2\pi f_p + \frac{2\pi}{\lambda}(a - \dot{d}(t_0)), -\frac{2\pi}{\lambda}\ddot{d}(t_0)]^\mathsf{T}$. The abovementioned system is discretized at a sampling interval of $T = N \cdot T_s$, also known as the subaccumulation period, where N is the number of subaccumulated samples. Let k denote the time index corresponding to $t_k = kT + t_0$. The discrete-time model of (6) can be expressed as

$$\boldsymbol{\theta}(k+1) = \mathbf{F}\boldsymbol{\theta}(k) + \boldsymbol{w}(k) \tag{7}$$

where $\mathbf{F} \triangleq e^{\mathbf{A}T}$ is the discrete-time state transition matrix and $\boldsymbol{w}$ is the discrete-time process noise vector, which is a zero-mean white sequence with covariance $\mathbf{Q} = q_{\tilde{w}} \int_0^T e^{\mathbf{A}t}\boldsymbol{b}(e^{\mathbf{A}t}\boldsymbol{b})^\mathsf{T} dt$.

B. Adaptive KF-Based Carrier Tracking

The adaptive KF-based tracking algorithm operates in a similar fashion to Costas loops, except that the loop filter is replaced with a KF, where the measurement noise variance is varied adaptively. Let $\hat{\boldsymbol{\theta}}(k|l)$ denote the KF estimate of $\boldsymbol{\theta}(k)$ given all the measurements up to time-step $l \leq k$, and $\mathbf{P}(k|l)$ denote the corresponding estimation error covariance. The initial estimate and its corresponding covariance are denoted by $\hat{\boldsymbol{\theta}}(0|0)$ and $\mathbf{P}(0|0)$, respectively, and are calculated as discussed in Section III-B4. The KF-based tracking algorithm steps are discussed as follows:

1) *KF Time Update:* The standard KF time update equations are preformed to yield $\hat{\boldsymbol{\theta}}(k+1|k)$ and $\mathbf{P}(k+1|k)$.

2) *KF Measurement Update:* The KF measurement update step is similar to a Costas loop: a carrier wipe-off is first performed, followed by an accumulation and discrimination step. The wipe-off and accumulation are performed as

$$s(k+1) = \frac{1}{N}\sum_{n=0}^{N-1} r(n+kN)\exp\left[-j\hat{\theta}(k+n|k)\right] \tag{8}$$

where $\hat{\theta}(k+n|k) = \hat{\theta}(k|k) + \hat{\dot{\theta}}(k|k)nT_s + \frac{1}{2}\hat{\ddot{\theta}}(k|k)(nT_s)^2$, which is obtained by propagating the initial condition $\hat{\boldsymbol{\theta}}(k|k)$ by nT_s using the dynamics in (6). Since the tracked signal in (3) is dataless, an atan2 discriminator can be used to obtain an estimate of the carrier phase error according to

$$\begin{aligned} \nu(k+1) &\triangleq \text{atan2}\left(\Im\{s(k+1)\}, \Re\{s(k+1)\}\right) \\ &= \theta(k+1) - \hat{\theta}(k+1|k) + v(k+1) \end{aligned} \tag{9}$$

where $\Re\{\cdot\}$ and $\Im\{\cdot\}$ denote the real and imaginary parts, respectively, and $v(k+1)$ is the measurement noise, which is modeled as a zero-mean, white Gaussian sequence with variance $\sigma_v^2(k+1)$. Since the measurement noise variance is not known, an estimate $\hat{\sigma}_v^2(k+1)$ is used instead in the KF. This estimate is updated adaptively according to the following section. It is important to note that $\nu(k+1)$ is the KF innovation and gives a direct measure of the modified beat carrier phase error. Hence, the standard KF measurement update equations are performed using $\nu(k+1)$, $\hat{\sigma}_v^2(k+1)$, and the measurement matrix $\mathbf{H} \triangleq [1\ 0\ 0]$.

3) *Measurement Noise Variance Estimate Update:* As the signal quality fluctuates, it is important to match the measurement noise variance to the actual noise statistics. This cannot be done readily as the channel between the LEO SV and the receiver is highly dynamic and unknown. Instead, a heuristic model is used to update $\hat{\sigma}_v^2(k)$ over time, and is given by

$$\hat{\sigma}_v^2(k+1) = \gamma\hat{\sigma}_v^2(k) + (1-\gamma)u(k) \tag{10}$$

where $0 < \gamma < 1$ is a "forgetting" factor (close to one) [11] and $u(k) \triangleq \frac{1}{K_v} \sum_{m=k-K_v+1}^{k} \nu^2(m)$, where K_v is the number of samples used to estimate the measurement noise variance. The heuristic model in (10) adapts to the quality of the measurements while filtering out abrupt changes in the phase error variance.

4) *KF Initialization:* The steps abovementioned assumed that an initial estimate and corresponding covariance are available. The initial estimate can be readily obtained from the data. Since a PLL cannot resolve the true initial carrier phase, the initial estimate $\hat{\theta}(0|0)$ is set to zero with zero uncertainty. This initial ambiguity is accounted for in the navigation filter. Initial estimates of the first and second derivatives of θ can be obtained by performing a search over the Doppler and the Doppler rate to maximize the FFT of the received signal. The search yields the Doppler and Doppler rate estimates denoted by $\hat{f}_D(0)$ and $\hat{\dot{f}}_D(0)$, respectively. In the following, let Δf_D and $\Delta \dot{f}_D$ denote the sizes of the Doppler and Doppler rate search bins, respectively. It is assumed that the initial Doppler and Doppler rate errors are uniformly distributed within one bin, and their initial probability density functions (pdfs) are bounded by Gaussian pdfs with zero-mean and standard deviations $\frac{\Delta f_D}{6}$ and $\frac{\Delta \dot{f}_D}{6}$, respectively. As such, Δf_D and $\Delta \dot{f}_D$ represent the $\pm 3\sigma$ intervals of the Gaussian pdfs. The KF is initialized as

$$\hat{\boldsymbol{\theta}}(0|0) = \left[0,\, 2\pi \hat{f}_D(0),\, 2\pi \hat{\dot{f}}_D(0)\right]^{\mathsf{T}} \tag{11}$$

$$\mathbf{P}(0|0) = \operatorname{diag}\left[0,\, \frac{4\pi^2}{36}\Delta f_D^2,\, \frac{4\pi^2}{36}\Delta \dot{f}_D^2\right]. \tag{12}$$

IV. EXPERIMENTAL RESULTS

This section provides the first results for carrier phase tracking and positioning with Starlink signals. To this end, a stationary National Instrument universal software radio peripheral (USRP) 2945R was equipped with a consumer-grade *Ku* antenna and low-noise block downconverter to receive Starlink signals in the *Ku*-band. The sampling bandwidth was set to 2.5 MHz and the carrier frequency was set to 11.325 GHz, which is one of the Starlink downlink frequencies. The samples of the *Ku* signal were stored for offline processing. The tracking results are presented in the following.

A. Carrier Phase Tracking Results

The USRP was set to record *Ku* signals over a period of 800 s. During this period, a total of six Starlink SVs transmitting at 11.325 GHz passed over the receiver, one at a time. The framework discussed in Section III was used to acquire and track the signals from these satellites with $\gamma = 0.99, K_v = 200, \Delta f_D = 250\,\text{Hz}, \Delta \dot{f}_D = 50\,\text{Hz/s}, q_{\tilde{w}} = (0.577)^2\ \text{m}^2/\text{s}^5$, and $\hat{\sigma}_v^2(0) = \frac{1}{9}(\frac{\pi}{2})^2\ \text{rad}^2$. The time history of $\nu(k)$ for each SV is shown in Fig. 2.

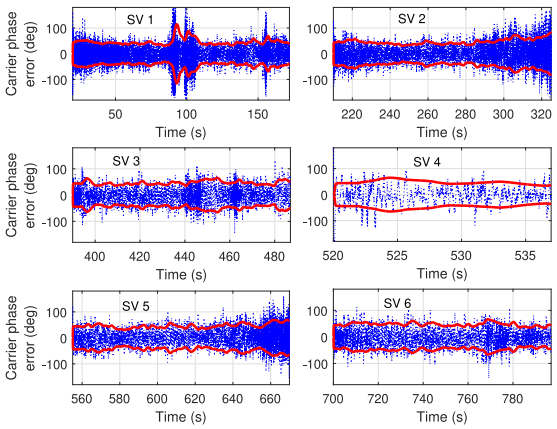

Fig. 2. Time history of $\nu(k)$ for each SV (dotted blue curves) and their corresponding $\pm 3\sigma$ bounds (solid red curves).

B. Position Solution

In the following, carrier phase observables are formed from the tracked modified beat carrier phases by (i) downsampling by a factor $D = 10$ to avoid large time-correlations in the carrier phase observables and (ii) multiplying by the wavelength to express the carrier observable in meters. Let $i \in \{1, 2, 3, 4, 5, 6\}$ denote the SV index. The carrier phase observable to the ith SV at time-step $\kappa = k \cdot D$, expressed in meters, is modeled as

$$z_i(\kappa) = \left\| \boldsymbol{r}_r - \boldsymbol{r}_{\text{SV}_i}(\kappa) \right\|_2 + a_i\, \kappa DT + b_i + c\, T_{\text{tropo},i}(\kappa) + v_{z_i}(\kappa) \tag{13}$$

where $\boldsymbol{r}_r$ and $\boldsymbol{r}_{\text{SV}_i}(\kappa)$ are the receiver's and ith Starlink SV 3-D position vectors expressed in an east-north-up frame centered at the receiver's true position; a_i and b_i are the coefficients of the first-order polynomial modeling the errors due to the initial carrier phase, clock bias, and unknown frequency shift f_p; c is the speed of light, $T_{\text{tropo},i}(\kappa)$ is the tropospheric delay for the ith SV; and $v_{z_i}(\kappa)$ is the measurement noise, which is modeled as a zero-mean, white Gaussian random variable with variance $\sigma_i^2(\kappa)$. The value of $\sigma_i^2(\kappa)$ is nothing but the first diagonal element of $\mathbf{P}(\kappa|\kappa)$, expressed in m^2. Tropospheric delay estimates $\hat{T}_{\text{tropo},i}(\kappa)$ are obtained using the Hopfield model [12] and subtracted from $z_i(\kappa)$ yielding the corrected measurement $\hat{z}_i(\kappa) \triangleq z_i(\kappa) - \hat{T}_{\text{tropo},i}(\kappa)$. In the following, define the parameter vector

$$\boldsymbol{x} \triangleq \left[\boldsymbol{r}_r^{\mathsf{T}}, a_1, b_1, \ldots, a_6, b_6\right]^{\mathsf{T}}. \tag{14}$$

Let $\hat{\boldsymbol{z}} \triangleq [z_1(0), \hat{z}_1(1), \ldots, \hat{z}_1(K_1), \ldots, \hat{z}_6(0), \hat{z}_6(1), \ldots, \hat{z}_6(K_6)]^{\mathsf{T}}$, where K_i denoted the total number of measurements from the ith SV, and let $\boldsymbol{v}_z \triangleq [v_{z_1}(0), v_{z_1}(1), \ldots, v_{z_1}(K_1), \ldots, v_{z_6}(0), v_{z_6}(1), \ldots, v_{z_6}(K_6)]^{\mathsf{T}}$, which is a zero-mean Gaussian random vector with a diagonal covariance $\mathbf{R}$ whose diagonal elements are given by $\sigma_i^2(\kappa)$. Then, one can readily write the measurement equation

$$\boldsymbol{z} = \boldsymbol{g}(\boldsymbol{x}) + \boldsymbol{v}_z \tag{15}$$

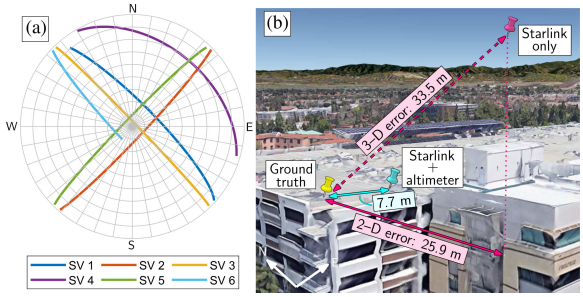

Fig. 3. (a) Skyplot showing the Starlink SVs' trajectories during the experiment. (b) Environment layout and positioning results.

where $\boldsymbol{g}(\boldsymbol{x})$ is a vector-valued function that maps the parameter $\boldsymbol{x}$ to the carrier phase observables according to (13). In the following, a weighted nonlinear least-squares (WNLS) estimator with weight matrix $\mathbf{R}^{-1}$ is solved to obtain an estimate of $\boldsymbol{x}$. The SV positions were obtained from TLE files and simplified general perturbation 4 software. It is important to note that the TLE epoch time was adjusted for each SV to account for ephemeris errors. This was achieved by minimizing the range residuals for each SV.

Subsequently, the receiver position was estimated using the aforementioned WNLS. The receiver position was initialized as the centroid of all SV positions, projected onto the surface of the earth, yielding an initial position error of 179 km. The clock biases and drifts were initialized to zero. The final 3-D position error was found to be 33.5 m, while the 2-D position error was 25.9 m. Upon equipping the receiver with an altimeter (to know its altitude), the 2-D position error goes down to 7.7 m. A skyplot of the Starlink SVs, the environment layout, and the positioning results are shown in Fig. 3.

V. CONCLUSION

This letter showed the first carrier phase tracking and positioning results with real Starlink LEO SV signals. A model of a Starlink SV's transmitted signal was formulated, and an adaptive KF-based carrier phase tracking algorithm was developed to track the Starlink signal. Experimental results showed carrier phase tracking of six Starlink LEO SVs over a period of approximately 800 s. The resulting positioning performance was: 7.7 m 2-D error when the receiver's altitude is known, and 25.9 m 2-D error and 33.5 m 3-D error when the receiver's altitude is unknown.

JOE KHALIFE, Member, IEEE
MOHAMMAD NEINAVAIE, Student Member, IEEE
ZAHER M. KASSAS, Senior Member, IEEE
University of California, Irvine, CA USA
The Ohio State University, Columbus, OH USA

REFERENCES

[1] D. Racelis, B. Pervan, and M. Joerger
Fault-free integrity analysis of mega-constellation-augmented GNSS
In *Proc. 32nd Int. Tech. Meeting Satellite Division Inst. Navigat.*, 2019, pp. 465–484.

[2] T. Reid *et al.*
Navigation from low earth orbit — Part 1: Concept, current capability, and future promise
In *Position, Navigation, and Timing Technologies in the 21st Century*, vol. 2, J. Morton, F. van Diggelen, J. Spilker Jr., and B. Parkinson, Eds. Hoboken, NJ, USA: Wiley, 2021, ch. 43, pp. 1359–1379.

[3] Z. Kassas
Navigation from low earth orbit — Part 2: Models, implementation, and performance
in Position, Navigation, and Timing Technologies in the 21st Century, J. Morton, F. van Diggelen, J. Spilker Jr., and B. Parkinson, Eds. Hoboken, NJ, USA: Wiley, 2021, vol. 2, ch. 43, pp. 1381–1412.

[4] M. Orabi, J. Khalife, and Z. Kassas
Opportunistic navigation with Doppler measurements from Iridium Next and Orbcomm LEO satellites
In *Proc. IEEE Aerosp. Conf.*, 2021, pp. 1–9.

[5] Z. Kassas, J. Khalife, M. Neinavaie, and T. Mortlock
Opportunity comes knocking: Overcoming GPS vulnerabilities with other satellites' signals
Inside Unmanned Syst. Mag., pp. 30–35, 2020.

[6] M. Neinavaie, J. Khalife, and Z. Kassas
Blind Doppler tracking and beacon detection for opportunistic navigation with LEO satellite signals
In *Proc. IEEE Aerosp. Conf.*, 2021, pp. 1–8.

[7] K. Kim, G. Jee, and J. Song
Carrier tracking loop using the adaptive two-stage Kalman filter for high dynamic situations
Int. J. Control, Autom. Syst., vol. 6, no. 6, pp. 948–953, 2008.

[8] L. Zhang, Y. Morton, and M. Miller
A variable gain adaptive Kalman filter-based GPS carrier tracking algorithms for ionosphere scintillation signals
In *Proc. ION Int. Tech. Meeting*, 2010, pp. 3107–3114.

[9] J. Won and B. Eisfeller
A tuning method based on signal-to-noise power ratio for adaptive PLL and its relationship with equivalent noise bandwidth
IEEE Commun. Lett., vol. 17, no. 2, pp. 393–396, Feb. 2013.

[10] J. Vila-Valls, P. Closas, M. Navarro, and C. Fernandez-Prades
Are PLLs dead? a tutorial on Kalman filter-based techniques for digital carrier synchronization
IEEE Aerosp. Electron. Syst. Mag., vol. 32, no. 7, pp. 28–45, Jul. 2017.

[11] Q. Xiang, Y. Yang, Q. Zhang, J. Cao, and Y. Yao
Adaptive and joint frequency offset and carrier phase estimation based on Kalman filter for 16 QAM signals
Opt. Commun., vol. 430, pp. 336–341, 2019.

[12] P. Misra and P. Enge
Global Positioning System: Signals, Measurements, and Performance, *2nd ed*. Kathmandu, Nepal: Ganga-Jamuna Press, 2010.